Statistical tomography of subkilometer irregularities in the high-latitude ionosphere

E. D. Tereshchenko

Polar Geophysical Institute of the Russian Academy of Sciences, Murmansk, Russia

M. O. Kozlova

Polar Geophysical Institute of the Russian Academy of Sciences, Murmansk, Russia

Now at Faculty of Physics, Moscow State University, Moscow, Russia.

V. E. Kunitsyn and E. S. Andreeva

Faculty of Physics, Moscow State University, Moscow, Russia

Received 15 November 2002; revised 6 October 2003; accepted 20 October 2003; published 24 January 2004.

[1] First results are reported on statistical tomography of kilometer-scale irregularities in the *F* layer high-latitude ionosphere from amplitude data of satellite radio probing. Basic formulae for statistical tomography of three-dimensionally (3-D) anisotropic small-scale irregularities are presented. It is shown that 3-D anisotropy disguises spatial distribution of irregularities but is not an insuperable difficulty for tomographic reconstruction. An example is shown of imaging the spatial distribution of the variance of electron density fluctuations over the Kola peninsula in February 1996. Iterative procedure of tomographic inversion was used in the reconstruction. Further steps of applying statistical tomographic approach are outlined. *INDEX TERMS:* 2407 Ionosphere: Auroral ionosphere (2704); 2439 Ionosphere: Ionospheric irregularities; 2487 Ionosphere: Wave propagation (6934); 6934 Radio Science: Ionospheric propagation (2487); 6984 Radio Science: Waves in plasma; *KEYWORDS:* statistical tomography, high-latitude ionosphere, kilometer-scale irregularities

Citation: Tereshchenko, E. D., M. O. Kozlova, V. E. Kunitsyn, and E. S. Andreeva (2004), Statistical tomography of subkilometer irregularities in the high-latitude ionosphere, *Radio Sci.*, *39*, RS1S35, doi:10.1029/2002RS002829.

1. Introduction to Theory

[2] Satellite radio tomography is known as an efficient method for mapping the structure of ionosphere [*Kunitsyn and Tereschenko*, 2003; *Pryse*, 2003; *Leitinger*, 1999]. This approach is based on the analysis of radio waves transmitted from flying satellite, then scattered by ionospheric irregularities, and measured by ground-based receivers. As the radio wave passes through the ionosphere, phase and amplitude of the signal change. Phase fluctuations are mostly due to large-scale irregularities with scale sizes much higher than the Fresnel radius. Spatial distribution of such irregularities can be reconstructed by means of ray radio tomography. The measured phase φ is proportional to the integral of electron density N along the ray s from a satellite to a receiver

$$\varphi \sim \int N ds. \tag{1}$$

[3] Phase measurements at a set of intersecting rays provide a linear system of integral equations like (1). Solving the system for N by means of tomographic inversion of the data yields the spatial distribution of electron density within the ionospheric volume under study.

[4] Scattering from small-scale irregularities with scale sizes of the order of, or less than, the Fresnel radius mostly contributes to amplitude fluctuations of radio waves. These irregularities may fill ionospheric volumes of various shapes and sizes so that the scattered field depends on a large set of scatterers and is therefore chaotic. Each separate irregularity cannot be investigated individually, and a statistical consideration is preferable.

0048-6604/04/2002RS002829

In this approach the ionosphere is regarded as a randomly inhomogeneous medium, and a relationship between statistical characteristics of the ionosphere and statistical parameters of the scattered radio wave is sought for.

[5] Consider a VHF radio wave scattered by electron density fluctuations of ionospheric plasma. Let inhomogeneous ionosphere be a plane layer, zL and zU being its lower and upper boundaries, respectively. Incident spherical wave is detected by a ground-based receiver. The z axis joins the source and the receiver and points in the direction of radio wave propagation. Coordinate $\vec{\rho}$ is transverse and perpendicular to z axis. The receiver is located at $\vec{r}_0$ (z_0, $\vec{\rho}_0$). Field $\vec{E}(\vec{r}, t)$ at a point $\vec{r}(z, \vec{\rho})$ within fluctuating ionosphere satisfies the equation

$$\mathrm{rot}\ \mathrm{rot}\vec{E} + \frac{1}{c^2}\frac{\partial}{\partial t^2}\vec{E} = -\frac{4\pi}{c^2}\frac{\partial}{\partial t}\hat{\sigma}\vec{E}, \tag{2}$$

where conductivity $\hat{\sigma}$ is a tensorial quantity and depends on various parameters of the medium denoted symbolically as ρ_i, $i = 0, 1, 2, \ldots$ In equation (2), t is time and c is the light velocity. In a fluctuating medium, each parameter can be represented as a sum of its mean value and deviation from the mean:

$$\rho_i = \langle \rho_i \rangle + \delta\rho_i.$$

[6] Angular brackets denote statistical averaging. If fluctuations are small, one can expand $\hat{\sigma}$ in a Taylor series and retain the first-order terms only:

$$\hat{\sigma} = \hat{\sigma}(\langle \rho_i \rangle) + \frac{\partial}{\partial \rho_i}\hat{\sigma}(\rho_i)|_{\delta\rho_i = 0}\delta\rho_i. \tag{3}$$

[7] Assuming $\langle \rho_i \rangle$ and $\delta\rho_i$ as time independent, the solution to equation (2) can be represented as a monochromatic wave

$$\vec{E}(\vec{r}, t) = \vec{E}(\vec{r})\exp(-i\omega t), \tag{4}$$

where ω is frequency.

[8] Assuming "cold" plasma approximation, conductivity tensor at frequencies not exceeding the hyrofrequency can be expressed as $\hat{\sigma} = \sigma\hat{I}$, where $\hat{I}$ is a unity tensor. Then

$$\sigma(\rho_i) = \frac{i\omega e^2(\langle N \rangle + \delta N)}{m\omega^2}, \tag{5}$$

where $\langle N \rangle$ is average electron concentration, δN electron density fluctuations, e electron charge, and m electron mass. Bearing in mind equations (3)–(5) and taking into account that in the absence of exterior charges $div\varepsilon\vec{E} = 0$ where ε is dielectric permittivity, one obtains equation (2) in the form

$$\nabla^2\vec{E} + k^2n^2\vec{E} = 4\pi\frac{e^2}{mc^2}\delta N\ \vec{E} + \mathrm{grad}(-\vec{E}\ \mathrm{grad}\ \varepsilon), \tag{6}$$

where $n = \sqrt{1 - \frac{\omega_p^2}{\omega^2}}$ is a refractive index, $\omega_p^2 = \frac{4\pi e^2\langle N \rangle}{m}$ is squared plasma frequency, and $k = \frac{2\pi}{\lambda}$ is wave number.

[9] In case of VHF waves propagation through the ionosphere the depolarization term grad$(-\vec{E}$ grad $\varepsilon)$ can be neglected [*Rytov et al.*, 1987]. Besides, the frequency of incident VHF wave is much higher than the plasma frequency; therefore one can assume $n \approx 1$. Taking into account $\frac{e^2}{mc^2} = r_e^2$ where $r_e = 2.82 \cdot 10^{-15}$ m^{-3} is classical electron radius, we obtain equation (6) in the form

$$\nabla^2\vec{E} + k^2\vec{E} = 4\pi r_e\delta N\vec{E}. \tag{7}$$

[10] Vector equation (7) splits into three scalar equations for field components E_x, E_y, and E_z,

$$\nabla^2 E + k^2 E = 4\pi r_e\delta N E, \tag{8}$$

which derives a relationship between amplitude of scattered field and the parameters of small-scale ionospheric irregularities. We shall use Rytov's approximation valid for comparatively weak scintillation. Solution to equation (9) can be present in the form

$$E = \exp(i\Psi(\vec{r})). \tag{9}$$

Substituting equation (9) into equation (8), expanding the solution of the obtained equation into a series of small parameter δN and grouping terms of the same order; we obtain a system

$$\begin{aligned} \nabla\Psi_0\nabla\Psi_0 - i\nabla^2\Psi_0 &= k^2 \\ 2\nabla\Psi_0\nabla\Psi_1 - i\nabla^2\Psi_1 &= -4\pi r_e\delta N \\ 2\nabla\Psi_0\nabla\Psi_n - i\nabla^2\Psi_n &= -\sum_{i=1}^{n-1}\nabla\Psi_i\nabla\Psi_{n-i}. \end{aligned} \tag{10}$$

[11] The first of these equations is a zero approximation that describes wave propagation through the medium containing no fluctuations. Subsequent equations describe wave interaction with fluctuations in the propagation medium. Assuming fluctuations to be weak, it is sufficient to consider only the first-order approximation and to solve an equation

$$2\nabla\Psi_0\nabla\Psi_1 - i\nabla^2\Psi_1 = -4\pi r_e\delta N. \tag{11}$$

With the solution in the form

$$\Psi_1 = U\exp(-i\Psi_0), \tag{12}$$

equation (8) appears as

$$\nabla^2 U + k^2 U = -4i\pi r_e \delta N \exp(i\Psi_0). \tag{13}$$

Solution to this equation is

$$U(\vec{r}) = ir_e \int_V d\vec{r}' \frac{\exp(ik|\vec{r}-\vec{r}'|)}{|\vec{r}-\vec{r}'|}\exp(i\Psi_0(\vec{r}'))\delta N(\vec{r}'). \tag{14}$$

Then

$$\Psi_1(\vec{r}) = ir_e \int_V d\vec{r}' \frac{\exp\left(ik|\vec{r}-\vec{r}'|\right)}{|\vec{r}-\vec{r}'|} \cdot \exp(i[\Psi_0(\vec{r}') - \Psi_0(\vec{r})])\delta N(\vec{r}'). \tag{15}$$

The solution to the equation of zero-order approximation is a spherical wave

$$\exp(i\Psi_0(\vec{r})) = A_0 \frac{\exp(ik|\vec{r}-\vec{r}_0|)}{|\vec{r}-\vec{r}_0|}, \tag{16}$$

where A_0 is amplitude of the wave. Taking into account equation (16), one obtains an expression for Ψ_1:

$$\Psi_1(\vec{r}) = ir_e \int_V d\vec{r}' \frac{|\vec{r}-\vec{r}_0|}{|\vec{r}-\vec{r}'||\vec{r}'-\vec{r}_0|} \cdot \exp\left(ik\left[|\vec{r}-\vec{r}'| + |\vec{r}'-\vec{r}_0| - |\vec{r}-\vec{r}_0|\right]\right)\delta N(\vec{r}'). \tag{17}$$

The field in the first-order Rytov's approximation can generally be described as

$$\vec{E} \approx \exp(i[\Psi_0(\vec{r}) + \Psi_1(\vec{r})]).$$

However, field $\vec{E}$ can be written as $\vec{E} = A(\vec{r})\exp(iS(\vec{r}))$, where A is amplitude and S is phase, whence it follows that

$$\chi = \ln\frac{A(\vec{r})}{A_0} = \mathrm{Re}(i\Psi_1(\vec{r})) = -r_e \int_V d\vec{r}' \frac{|\vec{r}-\vec{r}_0|}{|\vec{r}-\vec{r}'||\vec{r}'-\vec{r}_0|} \cdot \cos[k(|\vec{r}-\vec{r}'| + |\vec{r}'-\vec{r}_0| - |\vec{r}-\vec{r}_0|)]\delta N(\vec{r}). \tag{18}$$

[12] Here χ denotes logarithmic relative amplitude. Equation for the variance of log relative amplitude σ_χ^2 can be easily obtained from equation (18). Let $\vec{r}'(z', \vec{\rho}')$ and $\vec{r}''(z'', \vec{\rho}'')$ be current points of integration. Using paraxial approximation one arrives at

$$\begin{aligned}\sigma_\chi^2 &= \left\langle \ln\frac{A(\vec{r})}{A_0} \ln\frac{A(\vec{r})}{A_0}\right\rangle \\ &= \frac{r_e^2}{4}\int_Z^{Z_U}\int_Z^{Z_U} \frac{(z-z_0)^2 dz' dz''}{(z-z')(z'-z_0)(z-z'')(z''-z_0)} \\ &\cdot \int_{-\infty}^{\infty}\int_{-\infty}^{\infty} d\vec{\rho}' d\vec{\rho}'' \langle \delta N(r')\delta N(r'')\rangle \\ &\cdot \left\{ \exp\left[\frac{ik}{2}\left(\frac{|\vec{\rho}-\vec{\rho}'|^2}{z-z'} + \frac{|\vec{\rho}'-\vec{\rho}_0|^2}{z'-z_0} - \frac{|\vec{\rho}-\vec{\rho}_0|^2}{z-z_0}\right)\right] \right. \\ &\left. + \exp\left[-\frac{ik}{2}\left(\frac{|\vec{\rho}-\vec{\rho}'|^2}{z-z'} + \frac{|\vec{\rho}'-\vec{\rho}_0|^2}{z'-z_0} - \frac{|\vec{\rho}-\vec{\rho}_0|^2}{z-z_0}\right)\right]\right\} \\ &\cdot \left\{ \exp\left[\frac{ik}{2}\left(\frac{|\vec{\rho}-\vec{\rho}''|^2}{z-z''} + \frac{|\vec{\rho}''-\vec{\rho}_0|^2}{z''-z_0} - \frac{|\vec{\rho}-\vec{\rho}_0|^2}{z-z_0}\right)\right] \right. \\ &\left. + \exp\left[-\frac{ik}{2}\left(\frac{|\vec{\rho}-\vec{\rho}''|^2}{z-z''} + \frac{|\vec{\rho}''-\vec{\rho}_0|^2}{z''-z_0} - \frac{|\vec{\rho}-\vec{\rho}_0|^2}{z-z_0}\right)\right]\right\}. \end{aligned} \tag{19}$$

Converting to difference and summary coordinates $\vec{\mu} = \vec{\rho}' - \vec{\rho}''$, $\vec{\nu} = \frac{\vec{\rho}'+\vec{\rho}''}{2}$ and integrating over the summary coordinate $\vec{\nu}$, one obtains

$$\sigma_\chi^2 = \frac{2\pi^2 r_e^2}{k^2}\int_Z^{Z_U} K(0,z')dz' - \frac{\pi r_e^2}{2k}\int_Z^{Z_U}\frac{dz'(z-z_0)}{(z-z')(z'-z_0)} \cdot \int_{-\infty}^{\infty} d\vec{\mu}\, K(\vec{\mu},z')\sin\left(\frac{k(z-z_0)}{4(z-z')(z'-z_0)}|\vec{\mu}|^2\right), \tag{20}$$

where $K(\vec{\rho}, z) = \int_{-\infty}^{\infty}\left\langle \delta N(\vec{r}')\delta N(\vec{r}'')\right\rangle d(z'-z'')$ is correlation function of electron density fluctuations that is related to spectral density Φ_N by Fourier transform [*Ishimaru*, 1978]:

$$K(\vec{\rho}, z) = \frac{1}{(2\pi)^2}\int_{-\infty}^{\infty}\Phi_N(\kappa)|_{\kappa_z=0}\exp\left(i\vec{\kappa}_\rho\vec{\rho}\right)d\vec{\kappa}_\rho, \tag{21}$$

where κ_z and $\vec{\kappa}_\rho$ are wave vector components along and perpendicular to z axis, respectively. Substitution of equation (21) into equation (20) and integration of the obtained expression yields finally

$$\sigma_\chi^2 = \frac{\lambda^2 r_e^2}{4\pi^2}\int_Z^{Z_U} dz' \int_{-\infty}^{\infty} d\vec{\kappa}_{xy}\Phi_N\left(z'\vec{e}_z, \vec{\kappa}_{xy}\right)\sin^2\frac{R_F^2\kappa_{xy}^2}{4\pi}, \tag{22}$$

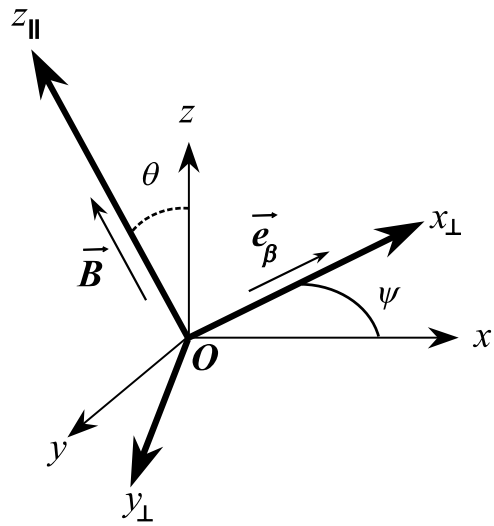

Figure 1. Coordinate systems associated with the direction of wave propagation and with the direction of geomagnetic field vector.

where λ is wavelength, $R_F = [\lambda z' \cdot (z' - z_0)/z_0]^{1/2}$ is the Fresnel radius, and $\vec{\kappa}_{xy} \equiv \vec{\kappa}_\rho$.

[13] Assuming that the same mechanism of irregularities generation operates all over the ionospheric region under study, spectral density can be written as

$$\Phi_N(\vec{\kappa}, z) = \sigma_N^2(z)\ \Phi_0(\vec{\kappa}, z), \tag{23}$$

where $\sigma_N^2(z)$ is a variance of electron density fluctuations that depends only on absolute value of z, and Φ_0 $(\vec{\kappa}, z)$ is normalized spectral density depending on the direction of $\vec{z}$. Applying to equation (22) the Kirchhoff formula linking the field in the fluctuating medium with the field outside, one obtains the equation for the variance of logarithmic relative amplitude at the receiving point:

$$\sigma_\chi^2 = \frac{\lambda^2 r_e^2}{4\pi^2} \int_{Z_L}^{Z_U} dz \sigma_N^2(z) \iint_{-\infty} d\vec{\kappa}_{xy} \Phi_0\left(z\vec{e}_z, \vec{\kappa}_{xy}\right) \sin^2 \frac{R_F^2 \kappa_{xy}^2}{4\pi}. \tag{24}$$

The double integral in equation (24) depends on the spectral shape only and not on the variance of electron density fluctuations.

[14] For further calculations the spectral shape should be specified. The power law spectrum is believed the most suitable model of ionospheric irregularities. High-latitude irregularities are known to be strongly anisotropic [*Aarons*, 1982]; therefore we shall use a model of 3-D anisotropic spectrum of irregularities elongated in the direction of geomagnetic field and in some field-perpendicular direction [*Fremow and Secan*, 1984].

$$\Phi_0(\kappa) = \frac{\alpha\beta L_0^3 \Gamma(p/2)}{2\pi\Gamma(3/2)\Gamma[(p-3)/2]} \cdot \left[1 + \left(\frac{L_0}{2\pi}\right)^2 \left(\alpha^2\kappa_\parallel^2 + \beta^2\kappa_{x\perp}^2 + \kappa_{y\perp}^2\right)\right]^{-p/2} \tag{25}$$

[15] Here α is relative elongation of irregularities in the direction of geomagnetic field vector $\vec{B}$, and β is relative elongation of irregularities in a plane perpendicular to the geomagnetic field (so as the irregularity axes relate as α: β: 1), Γ gamma function. $\kappa_\parallel$ is wave vector component parallel to the geomagnetic field, $\kappa_{x\perp}$ is a component in the direction of cross-field elongation of the irregularities, and $\kappa_{y\perp}$ is a component perpendicular to $\kappa_\parallel$ and $\kappa_{y\perp}$. Coordinate system used in equation (25) is portrayed in Figure 1 by thick lines. Since at small κ the factor $\sin^2 \frac{R_F^2}{4\pi}\kappa^2$ in equation (24) is of the order of κ^4, the contribution of large-scale irregularities with sizes exceeding the Fresnel radius is insignificant. Thus one can make use of the smallness of the Fresnel radius to outer scale ratio, and take the spectral shape as follows:

$$\Phi_{0(p)}(\kappa) = \frac{\alpha\beta L_0^3 \Gamma(p/2)}{2\pi\Gamma(3/2)\Gamma[(p-3)/2)]} \cdot \left[\left(\frac{L_0}{2\pi}\right)^2 \left(\alpha^2\kappa_\parallel^2 + \beta^2\kappa_{x\perp}^2 + \kappa_{y\perp}^2\right)\right]^{-p/2} \tag{26}$$

Finally, after integration of equation (24), we obtain for $0 < p < 4$ a formula for the variance of logarithmic relative amplitude of the wave scattered by 3-D anisotropic ionospheric irregularities

$$\sigma_\chi^2 = \frac{\lambda^2 r_e^2 \alpha\beta L_0^{3-p} \pi^{(p-1)/2}}{2^{3-p/2}\Gamma[(p-3)/2]\sin((p-2)\pi/4)} \cdot \int_{Z_L}^{Z_U} dz \frac{\sigma_N^2(z)}{\sqrt{1+\gamma(z)}} R_F^{p-2}(z) F\left[1 - \frac{p}{2}, \frac{1}{2}, 1, \frac{\gamma(z)}{1+\gamma(z)}\right] \cdot \left[C(z) - \sqrt{A^2(z) + B^2(z)}\right]^{-p/2}, \tag{27}$$

where

$$\gamma = \frac{2\sqrt{A^2(z) + B^2(z)}}{C(z) - \sqrt{A^2(z) + B^2(z)}}$$

$$A = \frac{1}{2}\left[\left(\alpha^2 - 1\right)\sin^2\theta(z) + \left(\beta^2 - 1\right) \cdot \left(\sin^2\psi\cos^2\theta(z) - \cos^2\psi\right)\right]$$

$$B = \left(\beta^2 - 1\right)\sin\psi\cos\psi\cos\theta(z)$$

$$C = 1 + \frac{1}{2}\left[\left(\alpha^2 - 1\right)\sin^2\theta(z) + \left(\beta^2 - 1\right) \cdot \left(\sin^2\psi\cos^2\theta(z) + \cos^2\psi\right)\right].$$

Here ψ is orientation angle of cross-field anisotropy, $\theta(z)$ an angle between the direction of wave propagation and the geomagnetic field vector, and F hypergeometric function. Coordinate system is oriented so that the geomagnetic field vector $\vec{B}$ is contained in yOz plane as shown in Figure 1 (thin lines). Unit vector $\vec{e}_\beta$ in the figure indicates the direction of cross-field elongation of irregularities.

[16] There is some specificity in application of the above equation to the analysis of experimental data. In a real experiment it is impossible to measure the field in the absence of irregularities. However, it turns out that within Rytov's approach an averaged measured amplitude $A_{0,e}$ can be successfully used instead of idealized quantity A_0. Let us show that an experimental estimate of the variance of logarithmic relative amplitude is identical to its theoretical value. Denote experimental logarithmic relative amplitude $\chi_e = \ln(A/A_{0e})$, where A is the measured amplitude and $A_{0e} = \langle A \rangle$ is experimental approximation of hypothetical amplitude in the medium containing no irregularities.

[17] Averaged amplitude $\langle A \rangle$ is linked with the amplitude of undisturbed field (in the absence of irregularities) A_0 by a relation [*Rytov et al.*, 1987]

$$\langle A \rangle = A_0 \exp\left(-0.5\sigma_\chi^2\right). \tag{28}$$

Making use of equation (28), we obtain

$$\chi_e = \ln\frac{A}{A_0 \exp\left(= -\sigma_\chi^2/2\right)} = \chi + \frac{\sigma_\chi^2}{2}, \tag{29}$$

where $\chi = \ln(A/A_0)$ is theoretical logarithmic relative amplitude. Averaging equation (29) and taking into account that $\langle \chi \rangle = -\sigma_\chi^2$ [*Rytov et al.*, 1987] gives

$$\langle \chi_e \rangle = -\frac{\sigma_\chi^2}{2}. \tag{30}$$

Finally, allowing for equality $\langle \chi^2 \rangle = \sigma_\chi^2 + \langle \chi \rangle^2$, we arrive at

$$\sigma_{\chi e}^2 = \left\langle \left(\ln\frac{A}{A_{0e}} - \left\langle \ln\frac{A}{A_{0e}} \right\rangle \right)^2 \right\rangle = \left\langle (\chi_e - \langle \chi_e \rangle)^2 \right\rangle = \sigma_\chi^2. \tag{31}$$

2. Applicability of Chosen Spectral Model to the Experimental Data

[18] The obtained equation (27) links the parameters of the scattering irregularities with the measured amplitude of the scattered radio wave and can serve as a good basis for investigation of small-scale ionospheric irregularities, provided the spectrum model adequately describes the experimental data. Equation (27) is obtained using Rytov's approximation valid for $\sigma_\chi{}^2 \leq 0.3$. This limiting condition is not too severe, and quite often it holds for experimental data. In order to verify practical applicability of the developed approach, a comparison has been made between theoretical and measured variance of logarithmic relative amplitude. Experimental data were obtained in a series of experiments carried out in 1997–1998 in the Murmansk region (northwest Russia) and in 1995 and 1997 in north Scandinavia. Receiving sites were located in a latitudinal interval from 68° to 70° N and covered different longitudinal regions in the auroral zone. The dates and sites of particular experiments are specified when describing the examples here below.

[19] In the experiments, 150 and 400 MHz radio signals from Russian navigation satellites were measured at chains containing three or four receivers. Orbit inclination of the satellites is 83° and their flight altitude about 1000 km. Receiving chains were oriented close to the ground projection of either upgoing (northward) or downgoing (southward) satellite flights. The length of a record was about 12 min (with 0.02 s data sampling) that is the time interval when satellite signal was kept locked by a receiver. The experimental data were processed as follows. The power index p was obtained from the high-frequency asymptote of experimental amplitude spectrum as shown in Figure 2. To calculate variance of log amplitude, the amplitude record of a given satellite pass was divided into a set of consecutive 10 s-long intervals shifted by 1 s. For each 10-s interval the variance of logarithmic relative amplitude was calculated. This value was attributed to the center of corresponding 10-s interval. The values thus calculated for all 10-s intervals plotted versus geographical latitude of the satellite. The obtained experimental dependencies were then fitted by theoretical model calculated from equation (27) by varying the values of anisotropy parameters (α, β, and ψ) until the best fit was approached. The initial values of

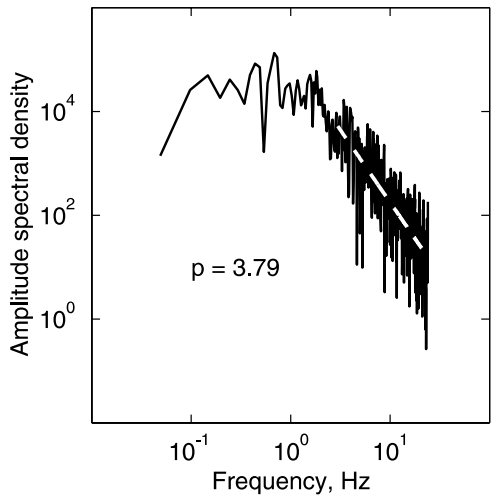

Figure 2. Determination of the power index from amplitude spectral density.

anisotropy parameters were chosen arbitrarily, then the theoretical curve was calculated and compared with the experimental one. After this we varied the values of anisotropy parameters in order to fit the location and the shape of the aspect maximum and the position of the "wings" of theoretical curve. Anisotropy parameters obtained from the best fit were considered as those describing the observed irregularities. In order to calculate theoretical curves, one should specify the model of spatial distribution of electron density fluctuations in the ionosphere. The simplest model suitable for slightly disturbed ionospheric conditions is a statistically homogeneous layer extending horizontally within a wide enough region. The layer was assumed 100 km thick, and its center in different models was at 250–350 km. Practical calculations were performed in geographic coordinates, which is more convenient in visualization the orientation of cross-field anisotropy. The latter can be represented as a sum of angle $\tilde{\psi}$ in a horizontal plane (where $\tilde{\psi}$ is the angle between ground projection of cross-field anisotropy and geographical north, measured eastward) and an angle ϕ in a vertical plane. In practical calculations the angle $\tilde{\psi}$ was specified, and the angle ϕ was determined from a condition of orthogonality of the cross-field anisotropy to the geomagnetic field direction at a given point. Geographical coordinate frame can be easily obtained from the system used in equation (27) by two rotations. The Jacobian of such coordinate transformation is unity; therefore equation (27) can be directly applied to calculations in geographical coordinates. Note that in high latitudes the "horizontal" orientation angle $\tilde{\psi}$ is indeed close to ψ because the high-latitude geomagnetic field is close to vertical, and the plane of cross-field anisotropy is therefore close to a horizontal one.

[20] Analysis of a large data set showed that in case of weakly disturbed ionosphere the power law spectrum model properly reproduces the experimental variance of logarithmic relative amplitude [*Tereshchenko et al.*, 1999]. Some examples of fitting the model to the experimental data are shown in Figure 3. Figure 3a portrays experimental (solid line) and theoretical (dashed line) curves of logarithmic relative amplitude measured in April 1997 at Verkhnetulomsky (68°35′ N, 31°45′ E), Murmansk region. Here and below the position of the receiving site is shown by a circle. As seen from the figure, the experimental variance has a single maximum caused by scintillation enhancement close to the geomagnetic zenith of the receiving site. The shape and location of the maximum depend on anisotropy parameters of irregularities and on the geometry of the experiment (on the position of satellite with respect to the vector of geomagnetic field). In Figure 3a the satellite trajectory lay very close to the geomagnetic zenith (minimum angle between the line-of-sight and the direction of local geomagnetic field vector was $\theta_{min} = 0.25°$). With this geometry the orientation of cross-field anisotropy of the irregularities has almost no effect on the shape and the position of $\sigma_\chi{}^2$ peak, and experimental curves can be reproduced by a model of irregularities symmetrical about the geomagnetic field. The best fit of the theoretical curve to the experimental one in the present case is observed at $\alpha = 45$.

[21] Figures 3b, 3c, and 3d display experimental and fitted theoretical curves calculated from the data measured (b) in April 1997 in Verknetulomsky, (c) in November 1995 in Esrange 67.89°N, 21.12°E, Sweden, and (d) in November 1995 in Trømso 69.59°N, 19.22°E, Norway. Theoretical curves calculated for the model of irregularities symmetric about the geomagnetic field (cross-field-isotropic) are shown by dashed lines, and those calculated for cross-field-anisotropic irregularities are shown by dotted lines. In these cases, satellites flew at some distances from the geomagnetic zeniths of the receiving sites: minimum angles between the line-of-sight and the geomagnetic field were (b) $\theta_{min} = 2.3°$, (c) 3.7°, and (d) 8.7°. In all these cases the experimental variance of logarithmic relative amplitude could no longer be reproduced by the model of irregularities symmetric in a plane perpendicular to the geomagnetic field since cross-field anisotropy of irregularities has an increasing effect on the amplitude variance curves with growing θ_{min}. The effect becomes noticeable starting from $\theta_{min} \approx 1° - 1.5°$. In Figure 3b the best fit of the model to the experimental curve is reached at $\alpha = 60$, $\beta = 7$, and $\tilde{\psi} = 87°$. In Figure 3c the best fit is encountered at $\alpha = 40$, $\beta = 10$, and $\tilde{\psi} = 80°$ and in Figure 3d at $\alpha = 38$, $\beta = 8$, and $\tilde{\psi} = 61°$. Generally, in all the cases shown, the

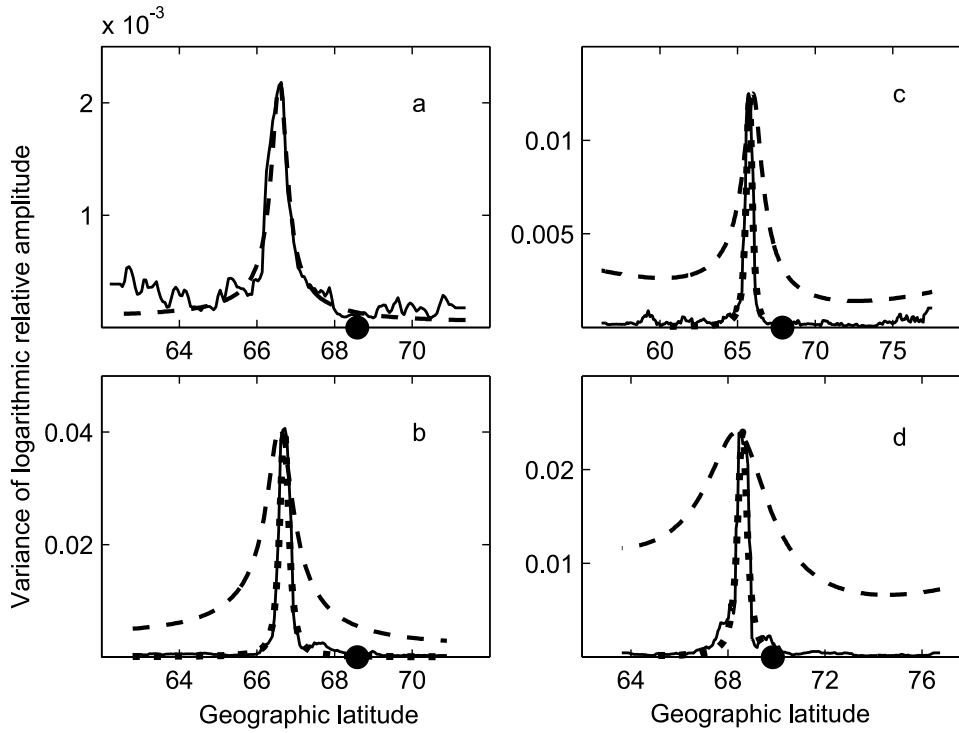

Figure 3. Fitting experimental variance of logarithmic relative amplitude by the model.

experimental data were properly fitted by the model if cross-field anisotropy was taken into account. Thus a good agreement between the experimental data containing a single aspect-due maximum and the fitted curves proves the applicability of the chosen spectral model to the analysis of amplitude scintillations of satellite radio signals.

3. Tomographic Approach

[22] The above analysis corresponds to the situation when the variance of density fluctuations remains constant within some ionospheric region. However, spatial uniformity over dozens to hundreds kilometers is not typical of high-latitude ionosphere. The structure of high-latitude ionosphere may undergo significant spatial and temporal changes owing to specific physical processes that take place in the near-polar regions. The assumption of constant spectrum seems still justified in many cases since the same generation mechanism hopefully operates in the whole region under study, while spatial changes in density fluctuations do often occur in the high-latitude ionosphere, which produces several maxima of various shape and magnitude in σ_χ^2. Some peaks in amplitude curve are due to the aspect effect; others reflect spatial variation in the distribution of electron density fluctuations which can be reconstructed from experimental data by means of tomographic approach. Indeed, the obtained integral equation

$$\sigma_\chi^2 \sim \int_{Z_L}^{Z_U} \sigma_N^2(z) \cdot f\{R_F, \theta, \alpha, \beta, \psi, p\} dz \qquad (32)$$

is structurally similar to equation (1) except for the additional weighting factor f reflecting the aspect effect described in the previous section. The presence of weighting factor disguises spatial distribution of density fluctuations. However, its influence is significant only within a narrow cone around the local geomagnetic zenith of the receiving site, and in many cases this effect can be easily estimated from experimental data. Let us make sure that outside the geomagnetic zenith the weighting factor is slowly varying (nearly constant) function at any feasible α and β in experiments of various geometries (for satellite passes at some distances from the local geomagnetic zenith with $\theta_{\min}$ varying from about zero up to dozen degrees). Figure 4 portrays latitudinal dependency of normalized variance of logarithmic relative amplitude $\sigma_\chi^2/(\sigma_\chi^2)_{\max}$ calculated for cross-field isotropic and cross-field anisotropic irregularities. In order to demonstrate the pure effect of the weighting function f, it is assumed that irregularities are distributed uniformly in a layer spreading horizontally

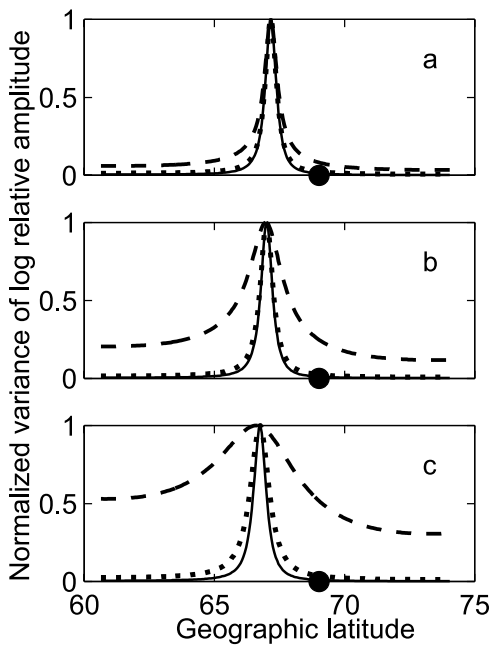

Figure 4. The effect of weighting function on normalized variance of logarithmic relative amplitude.

within wide enough region. The lower boundary of the layer is Z_L = 250 km, and its upper boundary Z_U = 350 km. Figure 4a portrays the case $\theta_{min} = 0.2°$ (nearly zenith satellite pass); in Figure 4b $\theta_{min} = 4°$, and in Figure 4c $\theta_{min} = 10°$. Orbital parameters of real satellite flights were used in the calculations. The power index p was 3.5. Calculations were made for the receiving point located at 69°01′N, 35°42′E, which is a site of regular measurements in the experiments performed by the Polar Geophysical Institute. Results for $\alpha = 30$ and $\beta = 1$ are shown by crosses, for $\alpha = 30$ and $\beta = 4$ by dots, and for $\alpha = 30$ and $\beta = 10$ by solid line. The orientation of cross-field anisotropy of the irregularities in all three cases was $\tilde{\psi} = 103°$.

[23] As seen from the figure, everywhere outside a comparatively narrow sector about the geomagnetic zenith the weighting coefficient is a smooth and slowly varying function. For $\theta_{min} < 2°$ the side "wings" of the curve are practically independent on β within a range $\beta = 2 \ldots 10$. For $\theta_{min} > 2°$ the off-zenith side parts of the curve only faintly depend on β as well. Thus, when making tomographic reconstruction, the weighting coefficients caused by anisotropy of irregularities should be taken into account only if probing rays intersect the ionospheric volume of interest close to geomagnetic zeniths of the receiving sites.

[24] Once the weighting function f is determined, the integral equation (27) becomes completely similar to equation (1), and the spatial distribution of the variance of electron density fluctuations can be reconstructed from amplitude measurements just in the same way as the electron density is recovered from the phase data in ray radio tomography.

[25] In tomographic experiments, each ionospheric volume in a vertical plane containing the receiving chain and the satellite path is consecutively illuminated by the rays from moving satellite to the receivers. If kilometer-scale irregularities are nonevenly distributed within this volume, the variance of electron density fluctuations can be reconstructed by means of tomographic method from the set of amplitude data measured along the probing rays that intersect the ionospheric volume (Figures 5a–5d). Note that the set of multireceiver data each containing a single aspect-due maximum (Figures 5e–5h) does not suit well for tomographic reconstruction This problem is equivalent to the reconstruction of spherically symmetric ionosphere (in ray tomography), which is difficult in practical implementation. Besides, the regions of maximum signal-to-noise ratio at different receiving sites are somewhat spaced apart; hence they do not form a system of intersecting rays (Figure 5h). In the left column the situation is sketched that fits well for tomographic reconstruction. The positions of receiving sites are shown by a circle, a square, and a triangle.

[26] Thus the data suitable for tomographic reconstruction of statistical structure of the ionosphere must meet the two requirements as follows: (1) the extrema in amplitude variance curves measured at different receiving sites should correspond to the same ionospheric volume containing irregularities of electron density fluctuations; that is, the probing rays should intersect within the volume with irregularities. (2) The extrema should come from the regions with high enough signal-to-noise ratio.

4. Reconstruction of Experimental Data

[27] The conditions formulated above are not too strict, and as the analysis of experimental data shows, they are often met in practice. Figure 6 shows experimental results obtained at 18:20–18:30 UT on 2 February 1996 at Kola peninsula. In this experiment, satellite radio signals> were measured at three receiving sites: Umba (66.69°N, 34.32°E), Lovozero (67.97°N, 35.02°E), and Tumanny (69.02°N, 35.7°E). The receiving chain was oriented along the ground projection of upgoing (northward) orbital circuits of the Russian navigational satellites.

[28] Solid lines in the figure show experimental variance of logarithmic relative amplitude of satellite radio signals measured in Umba (Figure 6a), Lovozero (Figure 6b), and Tumanny (Figure 6c). Each experimental curve contains several extrema. The most distinct peak in

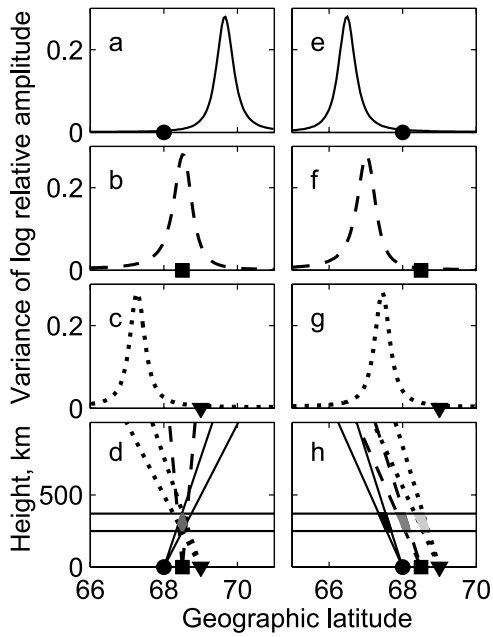

Figure 5. Aspect-due maxima favourable for tomographic reconstruction (left) and maxima badly suited for tomographic reconstruction (right).

Umba is located at 67.3°, somewhat to the north of the receiving site. A few of other maxima of lower magnitude are observed at 65°. . .66.5° to the south of the main maximum. In Lovozero, two separate maxima in amplitude variance are seen to the south of the receiving site. A larger maximum is observed at about 65.4°, and a smaller one is at approximately 66.5°. Both the extrema are smoother than those seen in Umba and Tumanny. The curve in Tumanny contains an isolated maximum at 67.5° to the south of the receiving site and also a rather wide zone of increased amplitude variance within latitudinal range 62°. . .64°. The northernmost separate extremum is comparatively smooth, but the southern area of increased amplitude variance is sharply indented. The magnitude of amplitude variance is nearly the same in both regions.

[29] The maxima located somewhat to the south of each receiving site are likely caused by geometrical enhancement of scintillation taking place close to local geomagnetic zeniths of the receiving sites. These aspect peaks are marked by "A" in the figure. The "aspect-due" maxima in all curves are reproduced, to some accuracy, by the same model of irregularities uniformly distributed within a 200 km thick spherical layer centered at a height of 280 km. Fitted curves are shown by dotted lines. Fitted anisotropy parameters are $\alpha = 40$, $\beta = 9$, and $\tilde{\psi} = 100°$.

[30] As seen in the figure, the theoretical curve properly reproduces the aspect-due experimental maximum in Lovozero. Similarly shaped experimental and theoretical aspect maxima in Tumanny are nearly collocated; however, their magnitudes do not match quite well. Less agreement is observed in Umba where the theoretical maximum does not match exactly any of experimental peaks but it falls well into an interval of increased amplitude variance. All of these discrepancies speak for spatial variations in the variance of electron density fluctuations in the ionosphere.

[31] There is another set of regions with increased amplitude variance (marked by "T") observed in all three experimental curves that correspond to the scattering from the same ionospheric volume. Once the spectrum of irregularities is determined from the aspect enhancement of scintillations, the spatial distribution of small-scale irregularities within this volume can be reconstructed from the amplitude variance data by means of the same procedure as in ray tomography, with σ_N^2 used instead of N.

[32] Each tomographic problem has its own specificity. For example, in ray tomography a problem exists of phase constant determination in linear integrals [*Kunitsyn et al.*, 1994, 1995]. Difficulties of other kind may arise in statistical tomography, such as some mismatch of the data from different receivers caused by a stochastic nature of the measured signals. Since the fluctuations of interest coexist with background fluctuations in the ionosphere, it is impossible to reconstruct absolute values of electron density fluctuations; only relative changes can be reconstructed.

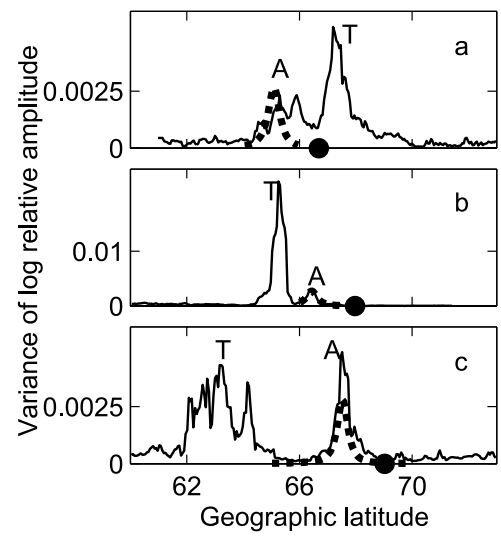

Figure 6. Experimental and model variance of logarithmic relative amplitudes measured at 18:20–18:30 UT on 2 February 1996 in (a) Umba, (b) Lovozero, and (c) Tumanny.

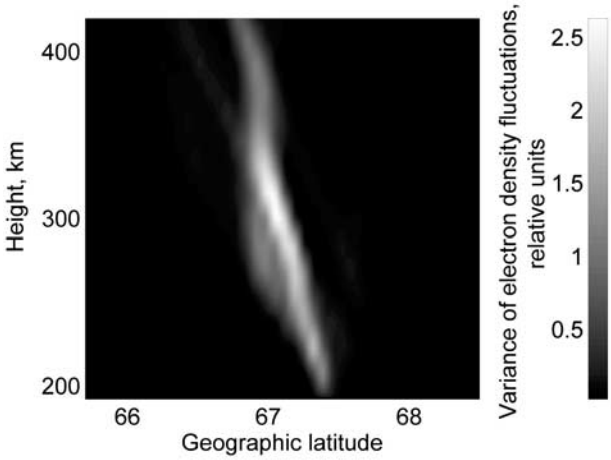

Figure 7. Tomographic image of relative changes in the variance of electron density fluctuations over Kola peninsula observed on 2 February 1996 at 18:20–18:30 UT.

[33] Usually it is hard to say which reconstruction techniques suit best for a particular case until the reconstruction is made. Which ones are preferable can be determined only from a numerical experiment. In the described case, optimum regularization parameters for the solution of the problem of statistical radio tomography were found as follows. Bilinear approximation within a grid cell 7.5 km long in latitude and 15 km high was applied in constructing the projection operator of the problem. The performed simulation showed that comparatively good reconstruction results are achieved if a combination of iterative algorithms is used such as algebraic relaxation technique (ART) applied to systems of inequalities as well, multiplicative algebraic reconstruction technique (MART), and decomposed algebraic reconstruction technique (DART) [*Kunitsyn et al.*, 1994, 1995].

[34] Figure 7 portrays the reconstruction (relative units) of relative changes in the variance of electron density fluctuations in the case described above. Relative errors (in C and L2 metrics) of the data from different receivers vary significantly. Whereas the Umba receiver has error levels of 12 and 15% (in C and L2, respectively) and Tumanny receiver of 25 and 24%, the middle receiver in Lovozero has much higher errors of 39 and 71%. Total error (for three receivers) is 39 and 34%. Big errors in L2 metrics in the Lovozero measurements are caused by the fact that these data have a very narrow peak of order of satellite shift by 1 degree, which corresponds to the fluctuating region 30 km wide at about 300 km height. The width of this peak is somewhat inconsistent with the data from other receivers. This discrepancy results in some widening of the projection of the function being reconstructed and produces big errors in integral metric.

[35] In the future it would be helpful to generate an assembly of the solutions of the statistical tomography problem [*Andreeva et al.*, 2001] and/or to estimate the obtained results using Bayessian approach [*Markkanen et al.*, 1995].

5. Summary

[36] For the first time, tomographic method is applied to reconstruction of statistical structure of electron density fluctuations in high-latitude ionospheric plasma. The analysis is based on measurements of satellite radio signals scintillation caused by scattering from kilometer-scale ionospheric irregularities. Applicability of the developed theory to the analysis of experimental data is proved by its comparison with amplitude measurements carried out in several experiments on Kola peninsula (northwest Russia) and in Scandinavia. It is shown that irregular spatial distribution of electron density fluctuations in the ionosphere indeed has a noticeable effect on the variance of logarithmic relative amplitude. Amplitude manifestations of nonuniform spatial distribution of density fluctuations are disguised by ''aspect-due'' maxima brought about by anisotropy of irregularities. If the ''aspect-due'' maxima in the variance of logarithmic relative amplitude are somewhat distant from those caused by variations in electron density distribution, the spatial distribution of the variance of electron density fluctuations can be reconstructed by tomographic method just like the structure of large-scale electron density irregularities is recovered from phase data in ray tomography. It should also be mentioned that the assumption of constant spectrum, generally, is not quite self-evident at distances of the order of hundreds kilometers. If the origin of a particular maximum in amplitude variance cannot be definitely ascertained, the regions of constant spectrum could be located by correlation measurements at one of the receiving sites, in addition to common satellite radio probing.

[37] **Acknowledgments.** The authors are grateful to Boris Khudukon for arrangement and carrying out the experiments on satellite radio probing in Scandinavia and at Kola peninsula.

References

Aarons, J. (1982), Global morphology of ionospheric scintillations, *Proc. IEEE*, *70*, 360–378.

Andreeva, E. S., S. J. Franke, K. C. Yeh, V. E. Kunitsyn, and I. Nesterov (2001), On generation of the assembly of images in ionospheric tomography, *Radio Sci.*, *36*, 299–309.

Fremow, E. J., and J. A. Secan (1984), Modeling and scientific application of scintillation results, *Radio Sci.*, *19*, 687–694.

Ishimaru, A. (1978), *Wave Propagation and Scattering in Random Media*, Academic, San Diego, Calif.

Kunitsyn, V., and E. Tereschenko (2003), *Ionospheric Tomography*, 272 pp., Springer-Verlag, New York.

Kunitsyn, V. E., E. D. Tereshchenko, E. S. Andreeva, and O. G. Razinkov (1994), Phase and phase-difference ionospheric radio tomography, *Int. J. Imag. Sys. Technol.*, *5*, 128–140.

Kunitsyn, V. E., E. S. Andreeva, A. Y. Popov, and O. G. Razinkov (1995), Methods and algorithms of ray radiotomography for ionospheric research, *Ann. Geophys.*, *13*, 1421–1428.

Leitinger, R. (1999), Ionospheric tomography, *Rev. Radio Sci., 1996–1999*, 581–623.

Markkanen, M., M. Lehtinen, T. Nygrén, J. Pirtilla, P. Henelius, E. Vilenius, E. D. Tereshchenko, and B. Z. Khudukon (1995), Bayesian approach to satellite radio tomography with applications in the Scandinavian sector, *Ann. Geophys.*, *13*, 1277–1287.

Pryse, S. E. (2003), Radio tomography: A new experimental technique, *Surv. Geophys.*, *24*, 1–38.

Rytov, S., Y. Kravtsov, and V. Tatarskii (1987), *Principles of Statistical Radiophysics*, vol. 2, Springer-Verlag, New York.

Tereshchenko, E. D., B. Z. Khudukon, M. O. Kozlova, and T. Nygrén (1999), Anisotropy of ionospheric irregularities determined from the amplitude of satellite signals at a single receiver, *Ann. Geophys.*, *17*, 506–518.

E. S. Andreeva, M. O. Kozlova, and V. E. Kunitsyn, Faculty of Physics, Moscow State University, Vorobjovy Gory, Moscow 119992, Russia. (andreeva@phys.msu.su; kozlova@phys.msu.su; kunitsyn@phys.msu.su)

E. D. Tereshchenko, Polar Geophysical Institute of the Russian Academy of Sciences, Khalturina Str. 15, Murmansk, 183010, Russia. (evgteres@pgi.ru)